Unique interplay between superconducting and ferromagnetic orders in EuRbFe$_4$As$_4$

V. S. Stolyarov,[1,2,3,*] A. Casano,[4] M. A. Belyanchikov,[1] A. S. Astrakhantseva,[1] S. Yu. Grebenchuk,[1] D. S. Baranov,[1,5]
I. A. Golovchanskiy,[1] I. Voloshenko,[4] E. S. Zhukova,[1] B. P. Gorshunov,[1] A. V. Muratov,[6] V. V. Dremov,[1] L. Ya. Vinnikov,[2]
D. Roditchev,[1,5,7] Y. Liu,[8] G.-H. Cao,[8,†] M. Dressel,[1,4] and E. Uykur[4,‡]

[1]*Moscow Institute of Physics and Technology, Dolgoprudny, Moscow 141700, Russia*
[2]*Institute of Solid State Physics (ISSP RAS), Chernogolovka 142432, Russia*
[3]*Kazan Federal University, 18 Kremlyovskaya Street, Kazan 420008, Russia*
[4]*1. Physikalisches Institut, Universität Stuttgart, D-70569 Stuttgart, Germany*
[5]*LPEM, ESPCI Paris, PSL Research University, CNRS, F-75005 Paris, France*
[6]*Lebedev Physical Institute, Russian Academy of Sciences, Moscow 119991, Russia*
[7]*Sorbonne Université, CNRS, LPEM, F-75005 Paris, France*
[8]*Department of Physics, Zhejiang University, Hangzhou 310027, China*

Transport, magnetic, and optical investigations on EuRbFe$_4$As$_4$ single crystals evidence that the ferromagnetic ordering of the Eu^{2+} magnetic moments at $T_m = 15$ K, below the superconducting transition ($T_c = 36$ K), affects superconductivity in a weak but intriguing way. Upon cooling below T_m, the zero resistance state is preserved and the diamagnetic response is only slightly affected by the emerging ferromagnetism; a perfect diamagnetism is recovered at low temperatures. The infrared conductivity is strongly suppressed in the far-infrared region below T_c, associated with the opening of a complete superconducting gap at $2\Delta = 10$ meV. A gap smaller than the weak-coupling limit suggests strong orbital effects or, within a multiband superconductivity scenario, the existence of a larger yet unrevealed gap.

New members of the iron-pnictide family, the so-called 1144 compounds, have attracted interest recently because the alternating layers of alkaline A and alkaline-earth B cations produce two different kinds of As sites [1–4]. These materials can be viewed as the intergrowth of A-122 and B-122 iron pnictides and they are naturally hole doped. The parent compounds are superconducting with transition temperatures T_c around 35 K, higher than most of the 122 materials; no spin-density-wave order has been observed. Among all possible candidates, Eu-based 1144 systems are even more intriguing, since the Eu sublattice orders ferromagnetically below a critical temperature $T_m \approx 15$ K [5,6], similar to the 122 counterpart EuFe$_2$As$_2$ [7–11]. Ferromagnetic order deep inside the superconducting state is very rare, in general [12,13]; hence the "ferromagnetic superconductor" EuRbFe$_4$As$_4$ might pave the way towards the realization of a "superconducting ferromagnet" [14–16]. However, the exact nature of the Eu magnetic order and its effect on superconductivity is unresolved [5,6] because single crystals have been synthesized only recently.

In this Rapid Communication we focus on the interplay between superconductivity and ferromagnetism in EuRbFe$_4$As$_4$ single crystals. We report comprehensive investigations comprising transport, magnetic, and optical measurements combined with microscopic studies of the vortex dynamics. The

infrared spectra show a clear gap opening around 80 cm^{-1} below $T_c = 36$ K that is slightly reduced compared to the value expected from the BCS theory. We relate this small value to the multiband character of superconductivity as well as to the depairing (orbital) effects of supercurrents screening the ferromagnetic domains. A surprisingly weak effect on the superconducting condensate has been observed upon magnetic ordering, indicating a rather weak interaction between Eu and Fe sublattices.

Single crystals of EuRbFe$_4$As$_4$ are obtained according to Refs. [4,5,17,18]; they exhibit shiny ab faces of approximately 1 mm in size. The structure of the compound is presented in Fig. 1(a). The crystals are characterized by x-ray, electrical transport, and magnetic susceptibility measurements. Our results are consistent with a recent independent study by Smylie and co-workers [19]. In Fig. 1(a) we plot the dc resistance versus temperature together with the $\omega \to 0$ extrapolation of the infrared (IR) measurements. The residual resistivity ratio (RRR) of 15.7 is significantly higher than reported for polycrystals [5,6]. The transition to the superconducting state takes place within a fraction of a degree [see the inset in Fig. 1(a)]. No effect of the ferromagnetic ordering at $T_m = 15$ K on resistivity is observed.

Figure 1(b) displays the temperature dependence of the magnetization probed in the field-cooling (FC) and zero-field-cooling (ZFC) protocol, for $H \parallel ab$ (black circles) and $H \parallel c$ (red triangles). The high quality of the crystals and the three-dimensional nature of the superconducting state are confirmed by the perfect diamagnetism rapidly reached below T_c for both field orientations. Below T_m the ferromagnetic ordering

---

*vasiliy@travel.ru
†ghcao@zju.edu.cn
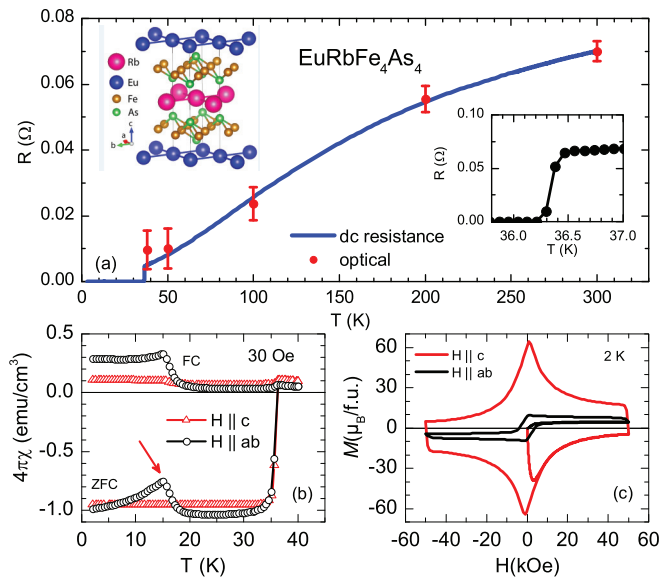‡ece.uykur@pi1.physik.uni-stuttgart.de

FIG. 1. (a) Temperature-dependent dc resistance (blue curve) of EuRbFe$_4$As$_4$ single crystals measured within the ab plane. The red dots correspond to the resistivity extracted from the Hagen-Rubens fit of the reflectivity normalized to dc resistance at room temperature, with $\rho = 0.23$ mΩ cm. The sharp superconducting transition at $T_c = 36.25$ K is magnified in the inset. The structure of the unit cell illustrates the two spacing layers: Eu in blue and Rb in magenta. (b) Magnetization at low temperatures measured by applying a magnetic field $H = 30$ Oe within the ab plane and perpendicular to it, $H \parallel c$. The phase transitions are indicated by a sharp drop at superconducting T_c and a pronounced feature around the magnetic order T_m, marked by a red arrow. The distinct behavior of field-cooled (FC) and zero-field-cooled (ZFC) susceptibility characterizes the superconducting state. (c) The completely different field-dependent magnetization for both orientations hallmarks the confinement of the magnetic moments to the ab plane.

FIG. 2. (a) Temperature evolution of the infrared reflectivity of EuRbFe$_4$As$_4$; at the lowest temperature the spectra approach unity around 80 cm^{-1}. The inset displays the overall behavior at ambient and low temperatures. (b) The corresponding conductivity spectra reveal the opening of the superconducting gap when the temperature drops below $T_c = 36$ K. The solid lines correspond to fits by the Drude-Lorentz model and Mattis-Bardeen equations, respectively. The left inset shows the complete behavior at $T = 300$ and 4 K. The right inset is the SW ratio in the normal state, indicating the SW transfer characteristics.

of the Eu sublattice gives a kinklike anomaly in magnetic susceptibility (indicated by the red arrow) that is only visible for $H \parallel ab$. The absence of ferromagnetic signature for $H \parallel c$ is taken as evidence that the ferromagnetic order of the Eu sublattice at $T_m = 15$ K results in domains oriented within the ab plane. The magnetization data presented in Fig. 1(c) confirm this conclusion: A pronounced hysteresis is observed within the plane, while the c-axis response is solely determined by the vortex dynamics [18]. The behavior is very much in contrast to the phenomena observed in the EuFe$_2$As$_2$ family where canted A-type antiferromagnetism dominates with a reentrant spin-glass behavior at lower temperatures [8–10].

The ab-plane optical reflection measurements are performed in a frequency range from 25 to 20 000 cm^{-1} and down to $T = 4$ K, using several Fourier-transform spectrometers complemented by IR microscopes and helium cryostats. The optical conductivity is obtained via the Kramers-Kronig analysis, using a Hagen-Rubens behavior in the normal state and Mattis-Bardeen fit in the superconducting state as low-frequency extrapolations; ellipsometric spectra collected up to 45 000 cm^{-1} and x-ray scattering functions were supplemented at higher frequencies. In Fig. 2 the IR reflectivity and conductivity are plotted for selected temperatures. At a first
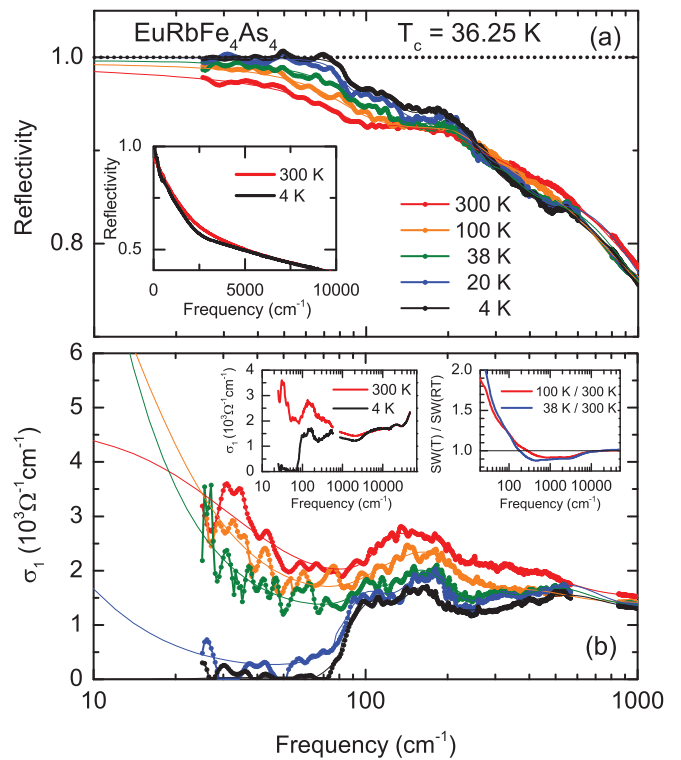
glance the overall optical response of this class of 1144 iron pnictide resembles that of the 122-type systems [20–24].

In the normal state, optical data presented in Fig. 2 can be described by two Drude components and a series of Lorentzians, as demonstrated in Fig. 3(a). The decomposition of the itinerant carriers into a narrow and a broad Drude (ND and BD, respectively) term accounts for the multiband scenario of iron pnictides [20,21]. Similar to the observations in Eu-based 122 compounds [7,25,26], the mid-IR band and higher-energy interband transitions are also visible. With decreasing T, the mid-IR absorption is suppressed and spectral weight is transferred to the higher energies [as seen in the inset of Fig. 2(b), the spectral weight (SW) ratio falls below "1" [27]]; we interpret this behavior as an indication of Hund's rule coupling [28]. The low-energy absorption features [orange bands in Figs. 3(a) and 3(b)] observed in EuRbFe$_4$As$_4$ are unique and their origin is not completely clear at this point. The temperature evolution of these bands summarized in Fig. 3(c) reveals the splitting below T_c and the redistribution at T_m.

The superconducting state is characterized by a distinct upturn of the reflectivity [29] reaching unity at around 80 cm^{-1}. As a consequence, the optical conductivity drops and

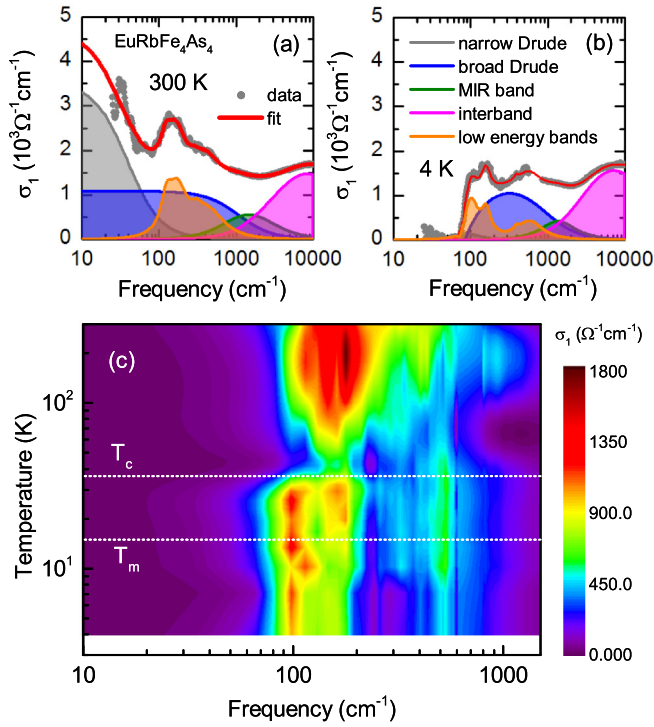FIG. 3. (a) Drude-Lorentz fits to the room-temperature optical conductivity of EuRbFe$_4$As$_4$. (b) In the superconducting state the two Drude modes are replaced by BCS terms [29]. Note the drastic changes in the low-energy bands. (c) The temperature and frequency dependences of the low-lying absorption modes highlight the effects of the phase transitions.

FIG. 4. (a) The superconducting gap of EuRbFe$_4$As$_4$ deviates from the prediction of a mean-field transition. (b) Temperature evolution of the superfluid density; the s-wave behaviors with different coupling constants are shown for comparison. A dip in the dependence is marked by a red arrow.

disappears for $\omega/(2\pi c) < 80$ cm^{-1} with basically no in-gap absorption. This evidences the presence of a complete gap throughout the Fermi surface, which might only have a small anisotropy [30]. The opening of the superconducting gap in $\sigma_1(\omega)$ can be well described by the Mattis-Bardeen equation [20,31] adding two contributions, corresponding to the Drude terms in the normal state; the result is summarized in the solid lines of Figs. 2(b) and 3(b). Here, one should note that the BD term dominates the gap structure and the contribution of the ND component is negligibly small. Moreover, within the error bars of the frequency scale, we cannot determine a significantly different gap value on the ND component. From the fits at 4 K we determine a gap value of $2\Delta_0 = (80 \pm 5)$ cm^{-1} = (10 ± 0.6) meV = $(3.17 \pm 0.2)k_B T_c$ that is about 10% below the predictions by the weak-coupling theory. The obtained frequency is in line with the small gap values detected for other 122 iron pnictides with a similar T_c [32,33]. Since in EuRbFe$_4$As$_4$ several electronic bands cross the Fermi level, one may expect other gap(s) to be present, having the ratio $2\Delta_0/k_B T_c > 3.53$ [34], similar to what is reported in 122 iron-based superconductors [32]. For CaKFe$_4$As$_4$ with $T_c = 31$–36 K, for instance, indications of two gaps, at 1–4 and 6–9 meV, have been reported [35]. The ND component of EuRbFe$_4$As$_4$, however, suggests that here we fall in the clean limit since $1/\tau_{nD} \approx 0.15\Delta$, while the BD term allows a small gap, $1/\tau_{bD} = 22\Delta$ [25,36].

It is remarkable that the gap $\Delta(T)$ in the IR spectra does not open gradually, as expected for a second-order transition,
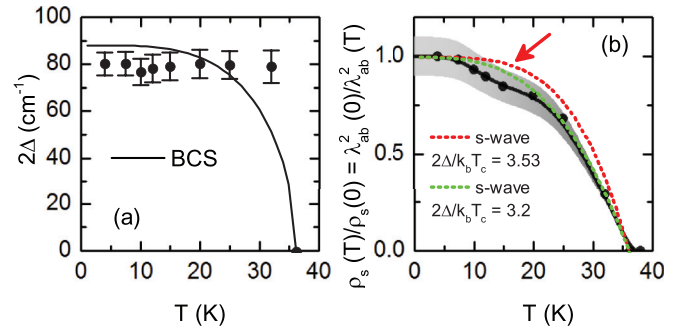
but rises sharply at T_c, as depicted in Fig. 4(a). Similar observations have been reported for other iron pnictides such as electron-doped Eu122 [26], Co-doped Ba122 [37], and Sm-1111 thin films [38]. Further theoretical effort is required to explain this behavior.

Upon the gap opening in the optical conductivity, the missing area $A = \int [\sigma_1^n - \sigma_1^s]d\omega$ between the normal and superconducting states, σ_1^n and σ_1^s, respectively, is condensed to the δ function at $\omega = 0$, according to the Ferrell-Glover-Tinkham sum rule [29]. Hence, the spectral weight analysis allows us to evaluate the penetration depth $\lambda = c/\sqrt{8A} \approx (420 \pm 45)$ nm at $T = 4$ K, comparable to similar iron pnictides, and the superfluid density $\rho_s(T) \propto 1/\lambda^2(T)$; the results are consistent with calculations based on the imaginary component $\sigma_2(\omega) \propto \Delta_0/\hbar\omega$. In Fig. 4(b), $\rho_s(T)$ is plotted together with predictions for s-wave gap symmetries with different coupling constants. Our results clearly deviate from the isotropic s-wave case (red line in the figure), while a smaller coupling constant can reproduce the results except for the dip feature marked with the red arrow. The sharp drop of the optical conductivity rules out the d-wave gap symmetry. Due to the observed temperature range, we attributed the dip feature to the effect of Eu ordering. We cannot rule out the possibility that this diplike feature is a result of the multiband nature of the sample [39], however, we think that the former explanation is more plausible, while we only observe one gap in the optical conductivity.

At first glance, there is no effect of the ferromagnetic order on the superconductivity of EuRbFe$_4$As$_4$. Indeed, unlike in Eu-122 systems, where reentrant superconductivity has been reported [26,40–42], we cannot detect any indication of ordering at T_m on the resistivity curve [Fig. 1(a)] or any noticeable in-gap absorption due to vortices in IR spectra; instead, a fully developed superconducting gap and s-wave characteristic of the superfluid density is observed. However, several signatures of the ferromagnetic order are unveiled by our investigations. First, the magnetization curve in Fig. 1(b) measured with a magnetic field within the ab plane shows a clear kink around $T = 15$ K—the perfect diamagnetism is destroyed; it is recovered only at significantly lower temperatures. Second, the superfluid density $\rho_s(T)$ in Fig. 4(b) manifests a weak dip in the range $T = 10$–15 K, followed
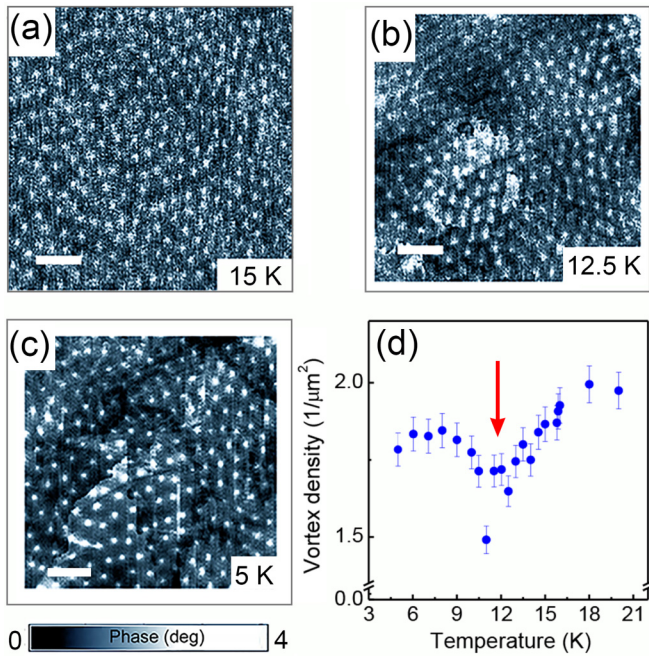
FIG. 5. Abrikosov vortex lattice in $EuRbFe_4As_4$ revealed by magnetic force microscopy. A field of $H = 35$ Oe is applied along the c direction, perpendicularly to the scanned sample surface. (a) For $T_m < T < T_c$ the main magnetic contrast comes from quite uniformly distributed vortices. (b), (c) For $T < T_m$ a large-scale magnetic contrast due to ferromagnetic domain walls adds to the vortex signal; the positions of the vortices are modified. The white scale bars correspond to 2 μm. (d) The temperature dependence of the vortex density integrated over the scanned area shows a minimum below the ferromagnetic transition, marked by a red arrow, followed by an increase at lower temperature.

by the recovery of superfluid density at lower temperatures (red arrow). Both experimental results suggest that the superconductivity is substantially weakened at the ferromagnetic transition but somehow "recovers" at lower temperatures.

This "weakening/recovery" of superconductivity in $EuRbFe_4As_4$ is confirmed by local magnetic force microscopy (MFM) investigations, in which the influence of ferromagnetic ordering on the Abrikosov vortex lattice is studied. Since the MFM probes the c component of the local magnetic field, the vortex lattice is created by applying an external field along the c axis of the crystal. The magnetic map in Fig. 5(a), acquired just above T_m, shows a lattice of Abrikosov vortices emerging out of the ab plane. The vortex organization, their surface density, and intervortex distances are typical of disordered type-II superconductors. The images displayed in Figs. 5(b) and 5(c) correspond to the same region of the sample; the maps were acquired at $T = 12.5$ K, right below T_m, and at $T = 5$ K, respectively. In these maps an additional magnetic contrast appears on a larger spatial scale, which is associated with a c-oriented component of the local field due the domain walls between neighboring ab-plane oriented ferromagnetic domains. The fact that the vortices continue to exist below T_m without any significant deformation of the vortex lattice evidences

a rather weak local field generated by the ferromagnetic domains. This behavior is in contrast to the stark effect of ferromagnetism on superconductivity observed in another ferromagnetic superconductor $EuFe_2(As_{1-x}P_x)_2$ in which a c-oriented ferromagnetic ordering takes place, leading to unique magnetic superconducting phases [43–45].

A detailed analysis of MFM data demonstrates that the ferromagnetic order does influences the vortex lattice, albeit weakly. This is demonstrated in Fig. 5(d) where the integrated vortex density is presented as a function of temperature. Above T_m, the vortex density is slowly reduced as the temperature is lowered, reflecting a continuous strengthening of superconductivity. Just below T_m this tendency slows down [red arrow in Fig. 5(d)], and then inverses. The observed increase in the vortex density below 12 K is associated with the weakening of the superconductivity by emerging ferromagnetism. Below 8 K, however, the superconductivity takes over again and the usual trend is restored. Notice that on a local scale, the vortex lattice becomes more inhomogeneous: Domains with unchanged vortex density coexist with regions where the density becomes significantly higher (in brighter areas) or lower (in darker areas), due to the spatially inhomogeneous out-of-plane component of the total field. This indicates that below T_m the vortex lattice is affected by ferromagnetism, but the intensity of the additional field remains rather low, as it is not able to significantly alter the vortex lattice. The weak coupling of ferromagnetism and superconductivity may imply the existence of rather weak exchange fields between the Eu and Fe sublattices, where such effects have been discussed previously for the Eu-122 systems with Eu bands located far away from the Fermi energy [46].

From our investigations on single crystals, we conclude that $EuRbFe_4As_4$ is a ferromagnetic multiband superconductor, in which superconductivity overcomes the ab-plane oriented ferromagnetic order of the Eu^{2+} ions. A single excitation gap at 80 cm^{-1} is observed below a sharp superconducting transition at $T_c = 36.25$ K; it reveals an unconventional temperature dependence. The gap energy $2\Delta_0 = 3.17 k_B T_c$ is below the weak-coupling limit, suggesting the existence of another larger superconducting gap. The reduction of the gap energy can also be associated with the depairing effect of spontaneous Meissner currents screening the ferromagnetic domains in the ab plane below T_m.

[1] H. Jiang, Y.-L. Sun, Z.-A. Xu, and G.-H. Cao, Chin. Phys. B **22**, 087410 (2013).

[2] K. Kawashima, T. Kinjo, T. Nishio, S. Ishida, H. Fujihisa, Y. Gotoh, K. Kihou, H. Eisaki, Y. Yoshida, and A. Iyo, J. Phys. Soc. Jpn. **85**, 064710 (2016).

[3] A. Iyo, K. Kawashima, T. Kinjo, T. Nishio, S. Ishida, H. Fujihisa, Y. Gotoh, K. Kihou, H. Eisaki, and Y. Yoshida, J. Am. Chem. Soc. **138**, 3410 (2016).

[4] Y. Liu, Y.-B. Liu, Q. Chen, Z.-T. Tang, W.-H. Jiao, Q. Tao, Z.-A. Xu, and G.-H. Cao, Sci. Bull. **61**, 1213 (2016).

[5] Y. Liu, Y.-B. Liu, Z.-T. Tang, H. Jiang, Z.-C. Wang, A. Ablimit, W.-H. Jiao, Q. Tao, C.-M. Feng, Z.-A. Xu, and G.-H. Cao, Phys. Rev. B **93**, 214503 (2016).

[6] Y. Liu, Y.-B. Liu, Y.-L. Yu, Q. Tao, C.-M. Feng, and G.-H. Cao, Phys. Rev. B **96**, 224510 (2017).

[7] D. Wu, N. Barišić, N. Drichko, S. Kaiser, A. Faridian, M. Dressel, S. Jiang, Z. Ren, L. J. Li, G. H. Cao, Z. A. Xu, H. S. Jeevan, and P. Gegenwart, Phys. Rev. B **79**, 155103 (2009).

[8] S. Zapf, D. Wu, L. Bogani, H. S. Jeevan, P. Gegenwart, and M. Dressel, Phys. Rev. B **84**, 140503 (2011).

[9] S. Zapf, H. S. Jeevan, T. Ivek, F. Pfister, F. Klingert, S. Jiang, D. Wu, P. Gegenwart, R. K. Kremer, and M. Dressel, Phys. Rev. Lett. **110**, 237002 (2013).

[10] S. Zapf and M. Dressel, Rep. Prog. Phys. **80**, 016501 (2017).

[11] M. Jannis and G. Philipp, Phys. Status Solidi B **254**, (2017).

[12] E. B. Sonin and I. Felner, Phys. Rev. B **57**, R14000 (1998).

[13] B. Lorenz and C.-W. Chu, Nat. Mater. **4**, 516 (2005).

[14] T. Nachtrab, C. Bernhard, C. Lin, D. Koelle, and R. Kleiner, C. R. Phys. **7**, 68 (2006).

[15] V. P. Mineev, Phys. Usp. **60**, 121 (2017).

[16] W.-H. Jiao, Q. Tao, Z. Ren, Y. Liu, and G.-H. Cao, npj Quantum Mater. **2**, 50 (2017).

[17] W. R. Meier, T. Kong, S. L. Bud'ko, and P. C. Canfield, Phys. Rev. Mater. **1**, 013401 (2017).

[18] Y. Liu and G.-H. Cao (unpublished).

[19] M. P. Smylie, K. Willa, J.-K. Bao, K. Ryan, Z. Islam, H. Claus, Y. Simsek, Z. Diao, A. Rydh, A. E. Koshelev, W.-K. Kwok, D. Y. Chung, M. G. Kanatzidis, and U. Welp, Phys. Rev. B **98**, 104503 (2018).

[20] D. Wu, N. Barišić, P. Kallina, A. Faridian, B. Gorshunov, N. Drichko, L. J. Li, X. Lin, G. H. Cao, Z. A. Xu, N. L. Wang, and M. Dressel, Phys. Rev. B **81**, 100512 (2010).

[21] N. Barišić, D. Wu, M. Dressel, L. J. Li, G. H. Cao, and Z. A. Xu, Phys. Rev. B **82**, 054518 (2010).

[22] M. Nakajima, S. Ishida, K. Kihou, Y. Tomioka, T. Ito, Y. Yoshida, C. H. Lee, H. Kito, A. Iyo, H. Eisaki, K. M. Kojima, and S. Uchida, Phys. Rev. B **81**, 104528 (2010).

[23] E. Uykur, T. Kobayashi, W. Hirata, S. Miyasaka, S. Tajima, and C. A. Kuntscher, Phys. Rev. B **92**, 245133 (2015).

[24] E. Uykur, T. Kobayashi, W. Hirata, S. Miyasaka, S. Tajima, and C. A. Kuntscher, Phys. Rev. B **95**, 214512 (2017).

[25] N. David, V. Pronin Artem, Z. Sina, M. Johannes, S. Jeevan Hirale, J. Wen-He, G. Philipp, C. Guang-Han, and D. Martin, Phys. Status Solidi B **254**, 1600148 (2017).

[26] A. Baumgartner, D. Neubauer, S. Zapf, A. V. Pronin, W. H. Jiao, G. H. Cao, and M. Dressel, Phys. Rev. B **95**, 174522 (2017).

[27] The spectral weight (SW) is obtained as $\frac{120}{\pi}\int_0^\omega \sigma_1(\omega)d\omega$. The cutoff value of ω is chosen through the entire measured range. The SW ratio, namely, SW(T)/SW(300 K), gives the characteristics of the SW transfers (transfer direction, energy scales, etc.). If there is a SW transfer from high to low energies (e.g., Drude narrowing), the ratio is above "1" at low energies and then approaches "1," and if there is a SW transfer from low to high energies, the ratio is below "1" until the full energy transfer is completed.

[28] A. A. Schafgans, S. J. Moon, B. C. Pursley, A. D. LaForge, M. M. Qazilbash, A. S. Sefat, D. Mandrus, K. Haule, G. Kotliar, and D. N. Basov, Phys. Rev. Lett. **108**, 147002 (2012).

[29] M. Dressel and G. Grüner, *Electrodynamics of Solids* (Cambridge University Press, Cambridge, UK, 2002).

[30] E. Schachinger and J. P. Carbotte, Phys. Rev. B **84**, 134522 (2011).

[31] B. Gorshunov, D. Wu, A. A. Voronkov, P. Kallina, K. Iida, S. Haindl, F. Kurth, L. Schultz, B. Holzapfel, and M. Dressel, Phys. Rev. B **81**, 060509 (2010).

[32] M. Dressel, D. Wu, N. Barišić, and B. Gorshunov, J. Phys. Chem. Solids **72**, 514 (2011).

[33] D. S. Inosov, J. T. Park, A. Charnukha, Y. Li, A. V. Boris, B. Keimer, and V. Hinkov, Phys. Rev. B **83**, 214520 (2011).

[34] H. Suhl, B. T. Matthias, and L. R. Walker, Phys. Rev. Lett. **3**, 552 (1959).

[35] P. K. Biswas, A. Iyo, Y. Yoshida, H. Eisaki, K. Kawashima, and A. D. Hillier, Phys. Rev. B **95**, 140505 (2017).

[36] Y. M. Dai, H. Miao, L. Y. Xing, X. C. Wang, C. Q. Jin, H. Ding, and C. C. Homes, Phys. Rev. B **93**, 054508 (2016).

[37] R. P. S. M. Lobo, Y. M. Dai, U. Nagel, T. Rõõm, J. P. Carbotte, T. Timusk, A. Forget, and D. Colson, Phys. Rev. B **82**, 100506 (2010).

[38] A. Charnukha, D. Pröpper, N. D. Zhigadlo, M. Naito, M. Schmidt, Z. Wang, J. Deisenhofer, A. Loidl, B. Keimer, A. V. Boris, and D. N. Basov, Phys. Rev. Lett. **120**, 087001 (2018).

[39] R. Prozorov and V. G. Kogan, Rep. Prog. Phys. **74**, 124505 (2011).

[40] C. F. Miclea, M. Nicklas, H. S. Jeevan, D. Kasinathan, Z. Hossain, H. Rosner, P. Gegenwart, C. Geibel, and F. Steglich, Phys. Rev. B **79**, 212509 (2009).

[41] U. B. Paramanik, D. Das, R. Prasad, and Z. Hossain, J. Phys.: Condens. Matter **25**, 265701 (2013).

[42] W.-H. Jiao, Y. Liu, Z.-T. Tang, Y.-K. Li, X.-F. Xu, Z. Ren, Z.-A. Xu, and G.-H. Cao, Supercond. Sci. Technol. **30**, 025012 (2017).

[43] I. Nowik, I. Felner, Z. Ren, G. H. Cao, and Z. A. Xu, J. Phys.: Condens. Matter **23**, 065701 (2011).

[44] I. S. Veshchunov, L. Y. Vinnikov, V. S. Stolyarov, N. Zhou, Z. X. Shi, X. F. Xu, S. Y. Grebenchuk, D. S. Baranov, I. A. Golovchanskiy, S. Pyon, Y. Sun, W. Jiao, G. Cao, T. Tamegai, and A. A. Golubov, JETP Lett. **105**, 98 (2017).

[45] V. S. Stolyarov, I. S. Veshchunov, S. Y. Grebenchuk, D. S. Baranov, I. A. Golovchansky, A. G. Shishkin, N. Zhou, Z. Shi,

X. Xu, S. Pyon, Y. Sun, W. Jiao, G.-H. Cao, L. Y. Vinnikov, A. A. Golubov, T. Tamegai, A. Buzdin, and D. Roditchev, Sci. Adv. **4**, 1 (2018).

[46] H. S. Jeevan, Z. Hossain, D. Kasinathan, H. Rosner, C. Geibel, and P. Gegenwart, Phys. Rev. B **78**, 052502 (2008).